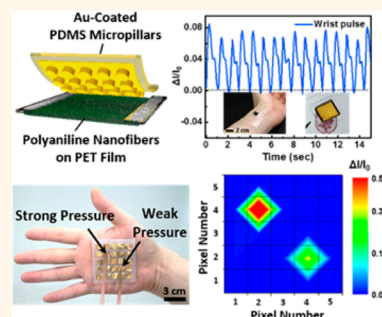# Stretchable Array of Highly Sensitive Pressure Sensors Consisting of Polyaniline Nanofibers and Au-Coated Polydimethylsiloxane Micropillars

Heun Park,[†] Yu Ra Jeong,[†] Junyeong Yun,[†] Soo Yeong Hong,[†] Sangwoo Jin,[‡] Seung-Jung Lee,[§] Goangseup Zi,[||] and Jeong Sook Ha*,[†,‡]

[†]Department of Chemical and Biological Engineering, [‡]KU-KIST Graduate School of Converging Science and Technology, and [||]School of Civil, Environmental and Architectural Engineering, Korea University, Seoul 136-701, Republic of Korea and [§]New Transportation Systems Research Center, Korea Railroad Research Institute, Uiwang-City, Gyeonggi-do 437-757, Republic of Korea

ABSTRACT We report on the facile fabrication of a stretchable array of highly sensitive pressure sensors. The proposed pressure sensor consists of the top layer of Au-deposited polydimethylsiloxane (PDMS) micropillars and the bottom layer of conductive polyaniline nanofibers on a polyethylene terephthalate substrate. The sensors are operated by the changes in contact resistance between Au-coated micropillars and polyaniline according to the varying pressure. The fabricated pressure sensor exhibits a sensitivity of 2.0 kPa^{-1} in the pressure range below 0.22 kPa, a low detection limit of 15 Pa, a fast response time of 50 ms, and high stability over 10000 cycles of pressure loading/unloading with a low operating voltage of 1.0 V. The sensor is also capable of noninvasively detecting human-pulse waveforms from carotid and radial artery. A 5 × 5 array of the pressure sensors on the deformable substrate, which consists of PDMS islands for sensors and the mixed thin film of PDMS and Ecoflex with embedded liquid metal interconnections, shows stable sensing of pressure under biaxial stretching by 15%. The strain distribution obtained by the finite element method confirms that the maximum strain applied to the pressure sensor in the strain-suppressed region is less than 0.04% under a 15% biaxial strain of the unit module. This work demonstrates the potential application of our proposed stretchable pressure sensor array for wearable and artificial electronic skin devices.

Recently, there has been a significant interest in the development of body-attachable electronic skin because electronic skin has potential applications as tactile, temperature, and vibration sensors.[1−7] To realize artificial skin, the precise measurement of pressure is considered to be one of the most basic and important requirements.[8,9] Pressure sensors usually operate as transducers that convert an applied force into an electrical signal or other recognized output signal. There are different types of transduction mechanisms, including piezoresistivity,[10−17] capacitance,[18−22] piezoelectricity,[23−26] and triboelectricity.[27−30] Among them, pressure sensors using the piezoresistive property have the advantage of a simple device structure and easy read-out mechanism when measuring the pressure caused by the variation in the resistance.[31]

In order to enhance the sensitivity of piezoresistive pressure sensors, i.e., increasing the rate of resistance change, various attempts have been made to optimize the structure and the materials: Maximizing the contact area can be achieved by performing structural modification such as the formation of a three-dimensional porous structure[12] or interlocked conductive array.[10,13] To improve the sensitivity, the selection of suitable materials including graphene,[32] carbon nanotubes,[19] metal nanowires,[16] and widely studied conductive polymers such as polypyrrole[33] and PEDOT:PSS[34] has also been proposed. In particular, conductive polymers have undergone extensive research because they can be easily synthesized and their conductivity can be tuned by doping and chemical treatment.[35] Even though the previously reported pressure sensor using

polypyrrole film showed a high sensitivity of 1.8 kPa^{-1} in the pressure range below 0.35 kPa, it could not detect pressures above 0.35 kPa because of the saturation of current.[33] Moreover, the fabrication of micropillar structure via photolithography of the silicon wafer and subsequent deep reactive ion etching made the process complicated and expensive. Recently, one-dimensional polyaniline nanofibers with ultrahigh surface area were reported to be easily formed using the potentiodynamic method.[36] The potentiodynamic synthesis has some advantages with regard to the mass production of nanofibers with uniform morphology and conductivity at room temperature. It is also possible to change the conductivity of the fiber film by controlling the thickness. Also, polyaniline nanofiber is environmentally stable, and its monomer is cost-effective.[37,38] Furthermore, this electrochemical polymerization method (*i.e.* potentiodynamic deposition method) does not include any surfactant or oxidant during the synthesis process which may contaminate the polyaniline samples and affect their electrical properties unless these are removed properly.[39]

In this study, we report on the facile fabrication of a stretchable array of highly sensitive pressure sensors. The proposed sensor is designed to satisfy both the structural and materials requirements that provide high sensitivity. The top surface of the sensor consists of Au-deposited PDMS micropillars, leading to high conductivity and the desired high sensitivity of the pressure sensor via optimization of the dimensions of micropillar array, while the bottom surface consists of conductive polyaniline nanofibers grown on a polyethylene terephthalate (PET) substrate by potentiodynamic method. The working principle of the sensor is related to a decrease in contact resistance between the top and the bottom surfaces under an applied pressure, and the large contact area between the interfaces due to the nanofiber structure of the polyaniline contributes to an enhancement in the sensitivity of the sensor. Furthermore, the air gap between those two layers enables a fast response and reduced relaxation time. As a result, the fabricated sensor showed a high sensitivity of 2.0 kPa^{-1} in the pressure range below 0.22 kPa, sensitivity with high linearity up to 1 kPa, a low detection limit of 15 Pa, and a fast response time of 50 ms at a low operating voltage of 1.0 V. In addition, electrical response to repetitive 10000 loading/unloading cycles of 1.5 kPa demonstrated the very highly reproducible performance of our sensor.

By integrating the fabricated sensors on a stretchable substrate using the dry transfer method, we also demonstrated its potential application as artificial skin. The stretchable substrate is composed of PDMS islands on which the individual pressure sensors are located and a mixed thin film of PDMS and Ecoflex between the adjacent islands. Pressure sensors are electrically connected with each other through the embedded liquid metal, Galinstan (68.5% Ga, 21.5% In, and 10% Sn), interconnections filling the microchannels in the mixed film of PDMS and Ecoflex. The integrated pressure sensor array showed very stable performance under an applied biaxial strain up to 15%, and the distribution of the strain corresponded to that estimated using finite element method (FEM) analysis. In addition to the excellent performance of the stretchable pressure sensor array, the whole fabrication process could be done simply and cost-effectively due to the use of molds for both the PDMS micropillars and the stretchable substrate. The SU-8 molds which was used to produce the PDMS micropillars could supply the micropillars semipermanently. That is, it was no longer required to perform a photolithography process once the SU-8 mold was fabricated. Furthermore, the stretchable pressure sensor array attached on the palm successfully detected the pressure, demonstrating its high potential for application to electronic artificial skin.

RESULTS AND DISCUSSION

Figure 1 illustrates the primary design concept of a biaxially stretchable pressure sensor array on a deformable substrate.

(1) Structure of a pressure sensor: We fabricated the pressure sensor by assembling the top layer of gold-deposited PDMS micropillars and the bottom layer of polyaniline nanofibers grown on a PET film, as shown in Figure 1a. We employed our specially fabricated Ag nanowire stickers as the electrodes for electrical measurements because they guaranteed the stable electrical performance of individual pressure sensors on the deformable substrate under stretching. This stable performance is attributed to the enhanced toughness of electrodes with numerous Ag nanowires, which reduces the concentration of stress near the electrical contact with the embedded liquid metal interconnections. The fabricated micropillar structure and polyaniline nanofibers are clearly confirmed by the scanning electron microscope (SEM images shown in Figure 1a. The detailed illustration of the fabrication of the pressure sensor will be discussed later.

(2) Sensing mechanism of the pressure sensor: Figure 1b shows the simplified electrical circuit of one row of PDMS micropillar array. In the circuit, R_{in} and R_{out} refer to resistances of the polyaniline nanofiber before and after the current flow through the Au-coated PDMS micropillars, which is located outside the pressure applied area, and R_C, R_{PANI}, and R_{Au} correspond to the contact resistance, the resistance of polyaniline nanofiber placed between two micropillars, and resistance of the Au film on the PDMS top substrate, respectively. The key operating mechanism of the sensor lies on the change in the contact resistance between the bottom surface of the PDMS micropillar and polyaniline nanofibers according to
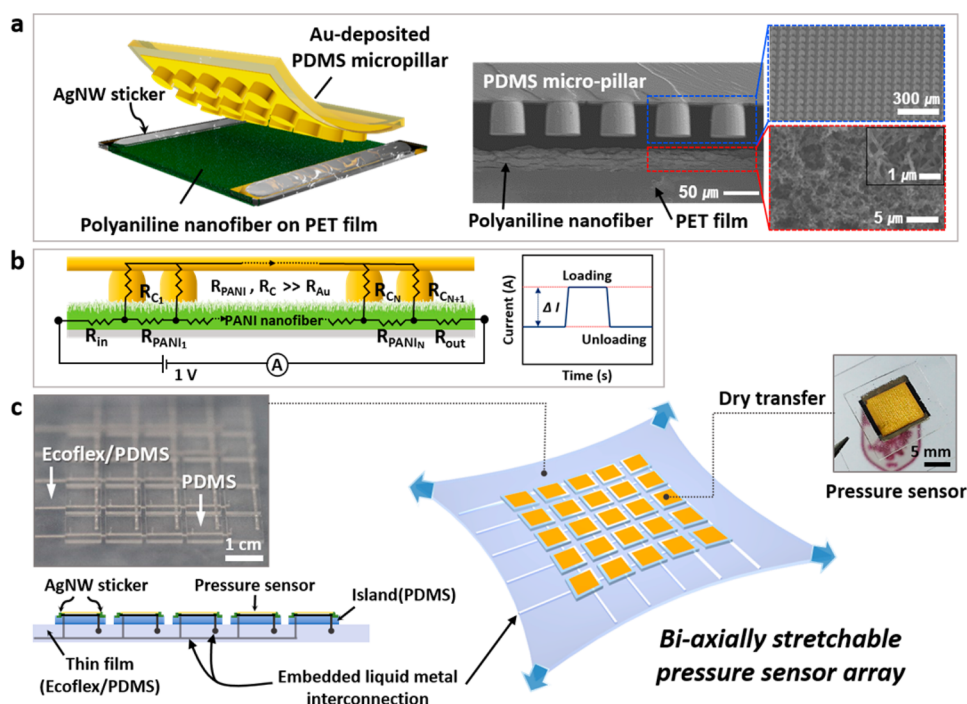
Figure 1. Primary design concept of biaxially stretchable pressure-sensor array on a deformable substrate. (a) (Left) Schematic illustration of a pressure sensor. (Right) Cross-sectional SEM image of the pressure sensor with zoomed SEM images of PDMS micropillars and polyaniline nanofiber film. (b) (Left) Schematic illustration of the sensing mechanism of the pressure sensor. (Right) Current changes in response to loading and unloading. (c) (Left) Optical image (top) and cross-sectional scheme (bottom) of deformable substrate consisting of rigid PDMS islands and soft thin-mixed film of PDMS and Ecoflex, where the electrical connection was made with embedded Galinstan interconnections. (Center) 5×5 array of pressure sensors on a stretchable substrate. (Right top) Optical image of the fabricated sensor.

the varying pressure. The total resistance of the sensor decreases as the contact resistance (R_C) decreases with vertically applied pressure. The roughness of the polyaniline nanofiber contributes to enhancing the sensitivity of the sensor. The higher the applied pressure to the sensor is, the lower the contact resistance becomes so that the most of the current would flow through the Au film coated on PDMS micropillars which have several orders of magnitude lower sheet resistance (0.03 Ω/sq) than that of polyaniline nanofiber film (sheet resistance = 420 $\pm$ 10 Ω/sq). Figure S1 presents cross-sectional SEM images of the sensor before and after loading compressive strain where the PDMS micropillars make contact with polyaniline nanofiber surface with pressure loading. It is observed that the pillars do not burrow into the polyaniline nanofiber film even when a larger magnitude of compressive pressure was applied to the sensor probably due to the difference in Young's modulus between the polyaniline nanofiber film and PDMS micropillars.[40,41]

(3) Fabrication of the stretchable sensor array: The fabricated pressure sensors were dry transferred onto a 5×5 array-structured stretchable substrate, where the sensors are electrically connected by embedded liquid metal interconnections, as shown in Figure 1c. The stretchable substrate is comprised of PDMS islands, on which the individual pressure sensors are located, and a thin mixed film of PDMS and Ecoflex between the

adjacent islands. The detailed fabrication of the stretchable substrate is illustrated in Figure S2.

In Figure 2, the fabrication and characterization of the pressure sensor are presented. To fabricate the top layer PDMS micropillar structure of the pressure sensor, microdot patterns were first prepared using the photolithography technique with SU-8 3050 negative photoresist, as shown in Figure 2a, where the inset shows the unit cell. Optical images of various dot patterns and unit cell sizes are also shown in Figure S3. Then, the liquid PDMS was poured into the patterned SU-8 mold and the cured PDMS layer was peeled off from the mold. The pillar has a diameter of 50 μm and a height of 48 μm. Pillar patterns with a diameter of 50 μm and a unit cell of 80×80 μm^2 are shown in Figure 2b. The detailed fabrication process is described in the Methods. Because the thickness of the SU-8 mold can be controlled by varying the spin-coating speed, the height of the PDMS micropillar can be varied accordingly. SEM images of the PDMS micropillar with various diameters and unit cell sizes are illustrated in Figure S4. The uniformity of the SU-8 film was confirmed from those images, which showed uniform size in diameter and height of pillars as well as straight edges of the micropillar walls. The Ti/Au (5/50 nm) film was deposited onto the fabricated PDMS micropillar via e-beam evaporation twice while the micropillar array was tilted 45° in the opposite direction to
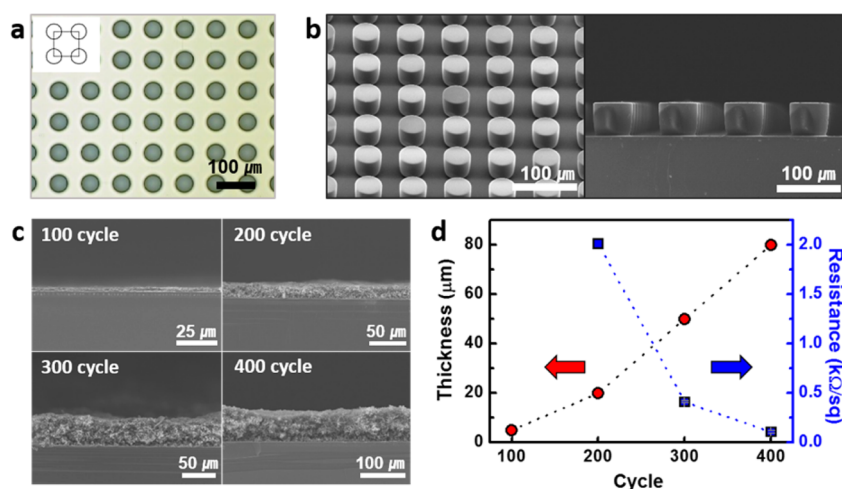
Figure 2. (a) Optical microscope image of SU-8 mold with dot patterns. The inset shows the unit cell. (b) Optical microscope image taken from (left) 45° tilted angle and (right) cross-sectional PDMS micropillar with a diameter of 50 μm and unit cell size of 80 $\times$ 80 μm^2. (c) Cross-sectional SEM images of polyaniline nanofiber film with different numbers of CV cycles. (d) Film thickness (red) and sheet resistance (blue) of electrodeposited polyaniline nanofiber film for 100, 200, 300, and 400 CV cycles.

obtain a uniform coating including the walls of the micropillars.

Polyaniline nanofibers were grown on a 50 nm thick Au-deposited PET film via the potentiodynamic method.[42] After 300 cycles of charging and discharging, we obtained a 50 μm thick film of polyaniline nanofiber with a diameter of $\sim$120 nm. Then, the Au layer was selectively etched away from the PET film so that only the polyaniline nanofiber film remained on a flexible PET substrate. The cross-sectional SEM images taken by varying the polyaniline growth cycles and the thickness-dependent sheet resistance of the grown film are shown in parts c and d, respectively, of Figure 2. The optimum thickness of the polyaniline film was chosen considering a reasonable conductivity value: The growth was not sufficient for less than 300 cycles, while the conductivity was too high to be used beyond the 300 cycles considering the relative difference in the conductivity between the polyaniline film and the top Au-coated micropillar layer. In addition, the final electrical conductivity of polyaniline nanofiber film could be determined by the ending potential of cyclic voltammetry (CV), since the electrical conductivity of polyaniline nanofiber prepared in the potentiodynamic method depends on its oxidation state, which is described in detail in Figure S5.

The growth of the polyaniline nanofiber film was also confirmed by taking the Fourier transform infrared (FT-IR) spectrum and Raman spectrum, as shown in parts a and b, respectively, of Figure S6. In the FT-IR spectrum, the bands at 1558 and 1476 cm^{-1} are assigned to be C=C stretching vibrations of quinoid and benzenoid rings, respectively. The bands at 1301, 1122, and 794 cm^{-1} originate from C–N, C=N, and C–H stretching vibrations, respectively.[43] The Raman peaks at 1160, 1332, 1488, and 1588 cm^{-1} are attributed to the C–H bending vibrations of quinoid rings,

C–N stretching vibrations, N–H bending vibrations, and the C=C bending vibration of benzenoid rings, respectively.[44] The cyclic voltammetry (CV) curves of the polyaniline nanofiber film with the variation of the deposition cycles are also shown in Figure S6c. With increase of the deposition cycles, the current increased indicating the continuous growth of polyaniline nanofiber film.

The electrical characteristics of the pressure sensor are presented in Figure 3. The custom-built device, which consisted of a computer-controlled positioning system and a force sensor, was designed to measure the response of the fabricated sensor to both dynamic and repetitive pressure loadings (Figure 3a). Figure 3b shows current–voltage curves of the pressure sensor under different pressure loading. The linear I–V curves exhibit Ohmic behavior. As the pressure loading increased, the current increased accordingly. Figure 3c shows the relative change in the current ($\Delta I / I_0$) through the sensor with the variation of the pressure loading, where I_0 and ΔI are the initial current and the change of current upon pressure loading, respectively.

According to Holm's theory,[33,45] the contact resistance (R_c) depends on the contacting area between two different materials as well as applied pressure following eq 1:

$$R_C(P) = k((P + P_{in})A_C)^{-n} \qquad (1)$$

Here, P, P_{in}, and A_C are applied pressure, initial pressure applied to the sensor due to the weight of the top PDMS substrate, and the area of the contacting surface in the direction of applied pressure, respectively. k and n are variables that depend on the device characteristics. In our pressure sensor, P_{in} is equal to zero since the top PDMS substrate is in a suspended state due to the thickness of the silver sticker. According to the above equation, the contact resistance decreases when contact
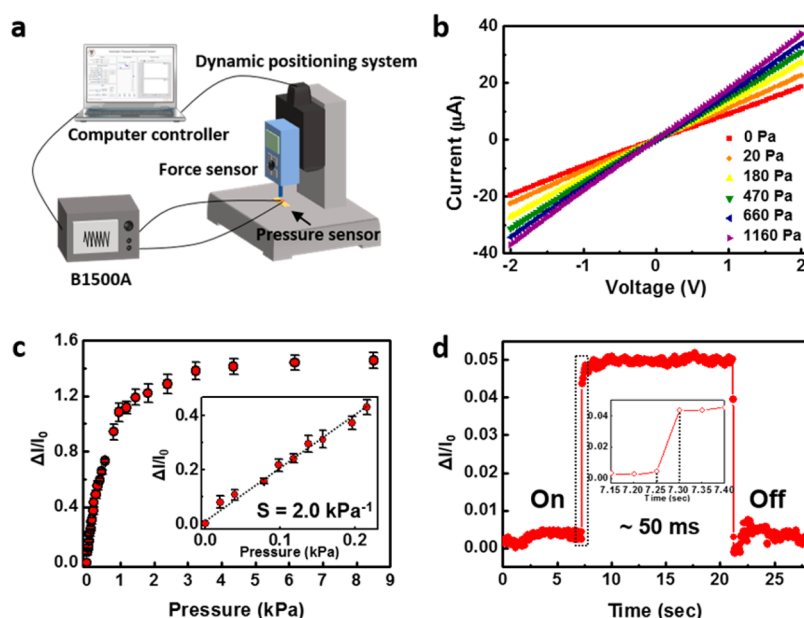
Figure 3. (a) Schematics of electromechanical measurement setup. (b) $I-V$ curves of the pressure sensor under different pressure loading conditions (0, 20, 180, 470, 660, and 1160 Pa). (c) Relative current change ($\Delta I/I_0$) *vs* applied pressure. The inset shows the zoomed pressure−response curve for values of pressure below 0.22 kPa with a sensitivity of 2.0 kPa^{-1}. (d) Response curve of the pressure sensor with an applied pressure of 20 Pa at a response time of 50 ms.

area is increased at constant pressure. This is because the compressive force applied onto the surface increases with increased contact area ($P = F/A$). In summary, the sensor detects external pressure due to the reduction in the contact resistance resulting from the applied pressure on the contact area between polyaniline nanofiber film and PDMS micropillars. The shape of the pressure dependent current change in Figure 3c exhibits the behavior following the above relationship. $\Delta I/I_0$ of the sensor changes rapidly with pressure in a low pressure regime, and it reaches saturation when the pressure is greater than a certain value ($P > 3.5$ kPa), showing an insignificant change in current.

Thus, $\Delta I/I_0$ increases linearly with the applied pressure in the low pressure region. The pressure sensitivity (*S*) is defined by eq 2,[16] indicating the slope in the linear region of the curve. Here, δP is the change in the applied pressure.

$$ S = \frac{\delta \frac{\Delta I}{I_0}}{\delta P} \quad (2) $$

As shown in the inset of Figure 3c, the sensitivity *S* exhibits the highest value of 2.0 kPa^{-1} with high linearity of $R^2 = 0.988$ with pressure of 0−0.22 kPa. Figure S7 shows the variation of the sensitivity depending on the applied pressure: an *S* value of 0.87 kPa^{-1} with excellent linearity of $R^2 = 0.998$ is given between 0.22 and 1 kPa (Figure S7a). In Figure S7b, a reduction of the sensitivity in the pressure between 1.0 and 3.5 kPa appears, but $\Delta I/I_0$ still shows the linear dependence with pressure ($R^2 = 0.966$) even considering the error bars. Above 3.5 kPa, however, the relative change in the

current seems to be almost saturated not to resolve the pressure quantitatively. The error bars in the graph represent the standard deviation obtained from averaging six devices.

As expressed in eq 1, the contact resistance also depends on the contact area between two different materials as well as the applied pressure.[33] By modifying the micropillar design using different pillar diameters and unit cell sizes, the sensitivity could be varied, as shown in Figure S8. Using a pressure sensor consisting of micropillars with a diameter of 120 μm and unit cell size of 160 × 160 μm^2, the highest total contact area was estimated, and it corresponded to the sensor with the highest sensitivity. The total contact area between PDMS micropillars and polyaniline nanofiber surface was calculated in the pressure applied regime (5 × 5 mm^2), and the relationship between the contact area and the sensitivity of the sensor is presented in Table S1. In Figure S9, the relative change in resistance is shown to increase with increasing contacting area under constant pressure. The change in resistance was saturated at contact areas of 7.9 and 12 mm^2, which is related to the power law relation between contact resistance and contact area as given in eq 1. These results suggest that the sensitivity of the pressure sensor be controlled by varying the dimensions of PDMS micropillar array.

Figure 3d shows the relative change in the current upon the application of a pressure of 20 Pa, and the inset indicates a fast response time of 50 ms. We compared the sensitivity, detection limit, and response time of our sensor with those reported previously for various pressure sensors in Table S2. The table shows
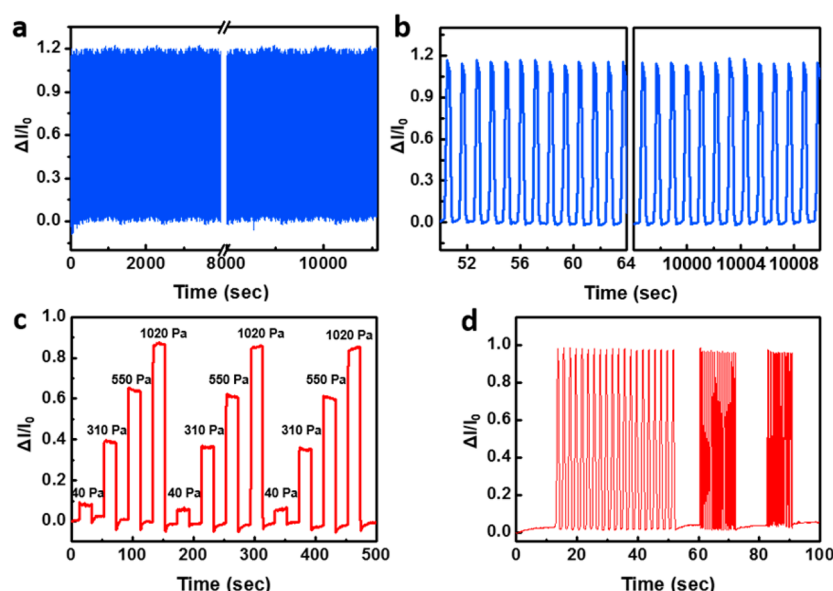
Figure 4. (a) Relative current change ($\Delta I/I_0$) of the sensor with repetition of 10000 loading/unloading cycles by 1.5 kPa. (b) Enlarged view of (a), exhibiting highly reproducible and stable sensor performance. (c) Repetitive measurements of the relative current change ($\Delta I/I_0$) of the sensor with variations of the pressure in a sequence of 40, 310, 550, and 1020 Pa. (d) Relative current change ($\Delta I/I_0$) under pressure loading of 1050 Pa at frequencies of 0.5, 1.7, and 2.5 Hz. I_0 and ΔI are the initial current and the change of current, respectively.

that the performance of our sensor is comparable to those selected from among the world's best sensors.

The response and relaxation curves of a pressure sensor measured for 10000 loading/unloading cycles of 1.5 kPa are shown in Figure 4a. During the large number of iterations, there appeared to be no difference in either the relative change of the current or the hysteresis, as clearly seen in Figure 4b. This demonstrates the very good reproducibility of our sensor. To investigate the reliability of the pressure sensor regardless of the magnitude of the applied pressure, we applied a series of pressures of 40, 310, 550, and 1020 Pa, and the same measurements were obtained three times. Over the wide range of applied pressures and repeated cycles, the current change remained almost the same as at the initial value within 3%, indicating that the sensor had excellent reproducibility (Figure 4c). Furthermore, we observed the stable detection of pressure, as shown in Figure 4d, regardless of the frequency of loading/unloading of pressure in the range between 0.5 and 2.5 Hz.

To determine the detection limit of our sensor, we repeatedly loaded and unloaded a very small grain of rice. Here, by assuming that it has an elliptical shape, the contact area of the 18 mg weighed rice is estimated to be ∼0.118 cm^2, which corresponds to a pressure of 15 Pa, as shown in Figure S10. Upon repetitive loading and unloading of the rice, increases and decreases of the current were repeatedly detected, demonstrating the high sensitivity of our sensor for a very small pressure (Figure 5a). Next, the fabricated sensor was attached to the carotid artery using a polyurethane film dressing (Tegaderm Absorbent, 3M), and the blood

pressure was measured. Time-dependent changes in the current show waves with a periodicity of 66 beats/min, confirming that it can detect the neck pulse of an ordinary human being (Figure 5b). In addition, the pressure sensor attached to the wrist of a female graduate student detected the periodic radial artery pulses in Figure 5c. The measured radial artery pulse exhibits two clearly distinguishable peaks (Figure 5d): systolic and diastolic peaks marked as "a" and "b", respectively. Important features such as the reflection index (R.I.) and stiffness index (S.I.) can be calculated as follows: (1) Reflection Index (R.I.) = magnitude of diastolic peak (b)/magnitude of systolic peak (a) × 100 (%) and (2) arterial stiffness index (S.I.) = subject height (h)/transit time (ΔT_{DVP}). The transit time (ΔT_{DVP}) is defined as the time delay between the systolic peak and diastolic peak.[46,47] The R.I. and S.I are estimated to be 51% and 4.2, respectively, indicating the healthy state of a 169 cm tall, 26 year old female.[48,49]

The pressure sensors were dry-transferred onto our specially designed stretchable substrate of a 5 × 5 array (Figure 6). In Figure 6a, the optical images of the integrated pressure sensor array before and after the application of biaxial stretching by 15% are shown. The substrate consists of a 5 × 5 array having 1 mm-thick protruded PDMS islands with a high Young's modulus where the 25 pressure sensors are positioned, and a 2.5 mm-thick mixed thin film of PDMS and Ecoflex with a weight mixing ratio of 2:8 with relatively low modulus due to soft Ecoflex component. The sensors were attached to the PDMS islands using thin Ecoflex adhesive film in order to minimize the strain applied to them under deformation.
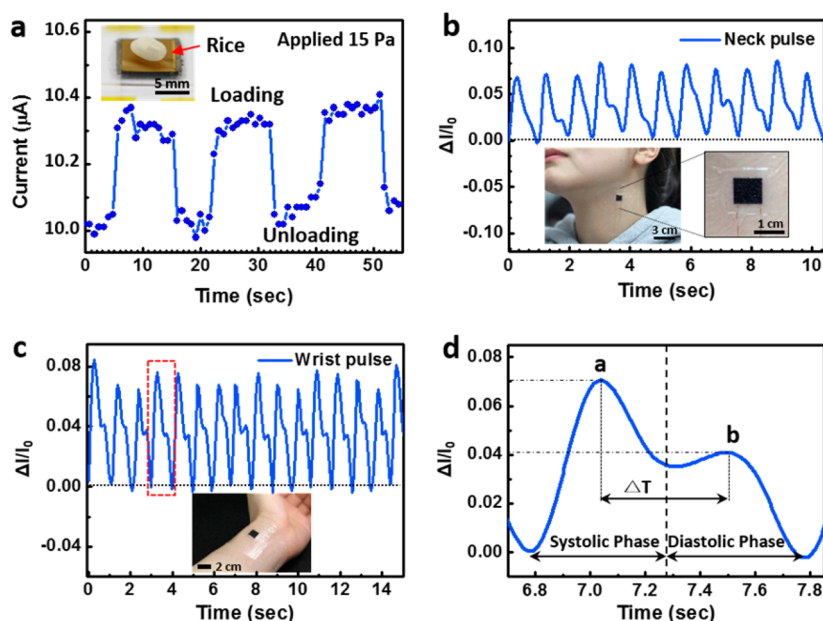
Figure 5. (a) Response and relaxation of the pressure sensor upon loading and unloading of a grain of rice with a pressure of 15 Pa, where the weight and the contact area of the rice are 18 mg and 0.118 cm^2, respectively. (b) Measurement of the neck pulse under normal conditions, indicating 66 beats/min. (c) Measurement of wrist pulse. (d) Zoomed waveform extracted from (c) showing some important features that are essential for health monitoring.
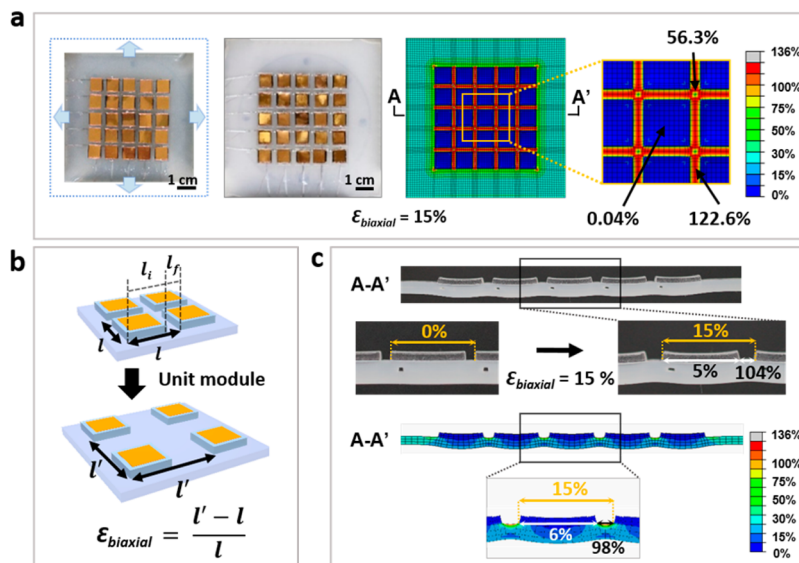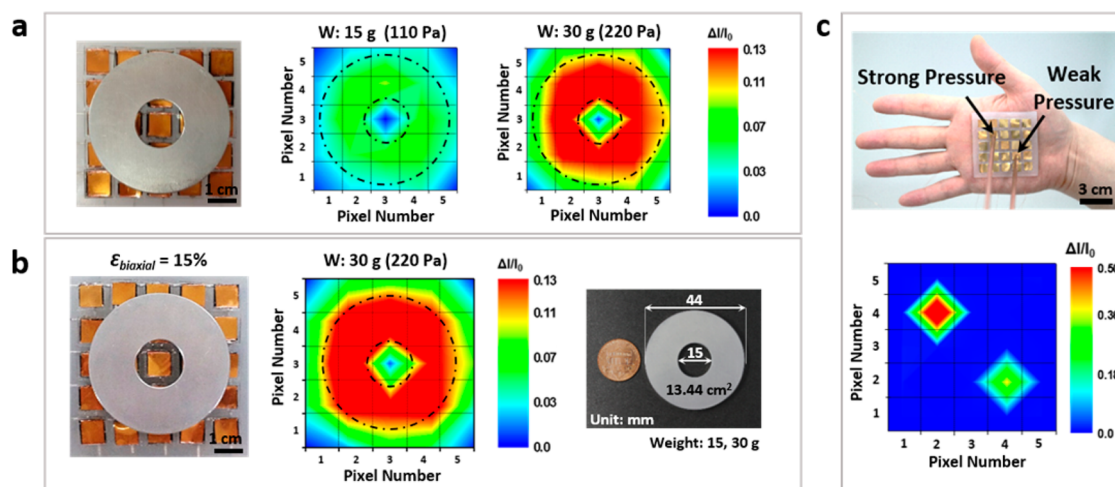

Figure 6. (a) Optical images of the pressure−sensor array on stretchable substrate (left) before and (second left) after application of the 15% biaxial strain. (Right) FEM analysis of the strain distribution on the stretchable substrate under biaxial strain of 15% with corresponding color scales of strain. (b) Schematic of definition of applied biaxial strain ($\varepsilon_{biaxial}$). (c) (Top) Cross-sectional optical image of the pressure sensor taken under 15% biaxial stretching, enlarged images (middle left) before and (middle right) after biaxial stretching by 15%. (Bottom) Corresponding distribution of strain estimated by FEM analysis under 15% biaxial stretching.

The distribution of the strain on the stretchable substrate calculated using the FEM method for a biaxial strain of 15% is shown in the right side of Figure 6a. The material properties for the substrates were modeled using the neo-Hookean model. The initial shear modulus and bulk modulus of PDMS are 2 and 200 MPa, respectively, and the values of mixed thin film are 0.4 and 40 MPa, respectively. The initial shear modulus and bulk modulus of the mixed thin film was calculated

as $G_{mix} = G_{PDMS}f_{PDMS} + G_{Ecoflex}f_{Ecoflex}$, where G is the initial shear and bulk modulus and f is the volume fraction.[50] The array of islands and thin film between the islands were modeled using the commercial finite-element program, ABAQUS.[51] The strain applied to the PDMS islands can be further suppressed by positioning a PET film on top of the islands because of the much higher Young's modulus of the PET film (3.1 GPa) relative to that of PDMS (615 kPa).[41] The PDMS islands

Figure 7. (a) (Left) Top-view image of the doughnut-shaped object placed on the 5 × 5 pressure-sensor array. Current mapping of pressure distributions with objects of (middle) 110 Pa and (right) 220 Pa. (b) (Left) Optical image of the sensor array under the biaxial strain of 15% with the doughnut-shaped object. (Middle) Current mapping of pressure distributions with object with a pressure of 220 Pa. (Right) Image of the doughnut-shaped object compared with a U.S. one-cent coin. (c) Current mapping on two different pressure sensors for different magnitudes of pressure.

with PET films hardly deform, and the deformation is concentrated on the thin film between two adjacent islands, as expected. On top of the island, the strain was just 0.04%, ensuring the stable performance of the pressure sensors on the islands.

In Figure 6b, the applied strain is defined as $\varepsilon_{biaxial} = (l' - l)/l$, where l and l' are the lengths associated with the unit module before and after application of strain, respectively. The cross-sectional optical microscope images of the stretchable substrate before and after biaxial stretching by 15% are shown in Figure 6c. About 5% of the strain was applied at the bottom of PDMS islands, while the strain over 100% was applied in the thin film between the islands. The strain contour that was estimated via FEM analysis is similar to that measured in the optical image. Human skin can be approximated as a bilayer film that consists of the epidermis (modulus = 140−600 kPa; thickness = 0.05−1.5 mm) and demis (modulus = 2−80 kPa; thickness = 0.3−3 mm). Because such a bilayer exhibits a linear elastic response to tensile strains ≤15%,[1] our stretchable sensor array, which can endure the 15% biaxial stretching, appears to have sufficient stretchability for use as an artificial skin device.

It was observed that the pressure sensor strongly depended on the stiffness of the substrate on which the sensor was deposited. In Figure S11, three different substrates with different Young's modulus were chosen to compare the sensitivity of the pressure sensor; a rigid glass substrate (50−70 GPa), PDMS substrate (615 kPa), and mixed-film substrate of PDMS and Ecoflex with mixing ratio of 2:8 (178 kPa). The Young's modulus of mixed-film substrate was calculated by the rule of mixture.[50] As a result, the sensor transferred to the rigid substrate showed the highest sensitivity, while on the polymer substrates, relatively low sensitivity was

obtained since the compressive force was transferred to the polymer substrate rather than being localized on the pressure sensor.

However, the stretchability of the sensor array as well as the sensitivity of the individual pressure sensor was considered when selecting the optimized composition of the deformable substrate. The extent of the stretchability was experimentally investigated by varying the mixing ratio of two different polymers of PDMS and Ecoflex and the stretchability increased with increasing the Ecoflex in our previous work.[41] As a result, the mixture of PDMS and Ecoflex with a mixing ratio of 2:8 was selected as an optimum substrate which met both the stretchability of the sensor array and the sensitivity of the pressure sensor.

In order to observe the distribution of the pressure on the 5 × 5 array of pressure sensors, a piece of doughnut-shaped aluminum (15 g, 110 Pa) was loaded as shown in Figure 7a. The color contrast mapped with the local pressure distribution is consistent with the shape of the doughnut. When the same sized object with twice the weight (30 g, 220 Pa) was placed on the sensor array, we observed the color contrast having the same distribution but with twice the intensity. This confirmed the reliable performance of the sensor array as a quantitative technique. Figure S12 shows spatial mapping of current changes and corresponding pressure on each pixel with loading of a doughnut-shaped aluminum piece (220 Pa). As clearly seen in Figure S12, each pixel gives a single value not to resolve different pressures within each pixel. However, we present each of the values as a contour line in Figure 7, analyzed using commercial software (Origin 9.0) to provide more specified and effective information on the pressure distribution. Figure 7b shows a similar intensity distribution with a corresponding shape even under 15% biaxial stretching.

In order to see if there exists any interference among the individual pressure sensor pixels in our stretchable sensor array, we checked the current change on the pixel (3, 3) on which no pressure was applied while the neighboring pixels were under pressure. Four different measurements were done for this: loading of doughnut-shaped aluminum pieces with 110 and 220 Pa, touching with two rods, and loading of 220 Pa doughnut-shaped aluminum under 15% strain, respectively. In all cases, the relative current change on the pixel (3, 3) was less than 0.5%, which was negligible as shown in Figure S13, suggesting no evidence of interference between the individual pressure sensor pixels within the experimental error range.

These results demonstrate the potential application of our pressure-sensor array as a body-attached device that can simultaneously detect both the pressure and shape of an object under conditions involving body movements such as bending or stretching. The sensor array that was attached on the right palm using the silicon adhesive, Silbione (Silbione RT Gel 4717 A&B, Bluestar Silicones, USA), is shown in Figure 7c. When a rod touched two different pixels above the pressure−sensor array with different pressures, we obtained the resolved mapping of the touching positions for the corresponding pressures.

There are many advantages of our work aside from the great electrical performances of the pressure sensor. First, we could control the sensitivity of our sensor through manipulation of the dimensions of micropillar array and could afford the high sensitivity using nanofibers with large surface area. In addition, environmentally stable polyaniline nanofibers could be produced on a large scale via a simple method with low cost. It was also easy to control the conductivity by adjusting the thickness and oxidation state of polyaniline nanofiber through electrochemical polymerization. Lastly, this is the first demonstration of fabricating pressure sensor array on the stretchable substrate using liquid metal interconnection, and it presents possibilities of skin-attached electronic application.

Even though we demonstrated successful performance of a stretchable pressure sensor array, there still remain several points to be improved by further research. First, it will be desirable to fabricate the sensor that has wider pressure range with a single high sensitivity. Second, the size of our pressure sensor (9×9 mm^2) needs to be reduced to obtain better spatial resolution. Third, total thickness of our sensor array (3.5 mm) is too thick to be directly attached to skin without using glue: The stretchable substrate with protruding PDMS islands for pressure sensors increases the thickness. Thus, further development of novel stretchable design and materials with sticky properties should be done. Lastly, although liquid metal was confirmed as a good material for stretchable electrical interconnection, more advanced fabrication technique such as printing rather than injection method should be developed to obtain more complicated designs.

METHODS

Fabrication of SU-8 Mold and Au-Deposited PDMS Micropillars. The fabrication scheme of the SU-8 mold and PDMS micropillars is presented in Figure S14a. The mold was prepared with a negative photoresist (PR) coated on a silicon substrate. SU-8 3050 photoresist is a highly viscous epoxy material that is useful for making high aspect-ratio structures. First, a 48 μm thick SU-8 3050 PR was spin coated on a SiO$_2$/Si substrate via the two-step spin-coating processes at 500 rpm for 10 s and subsequently at 3000 rpm for 30 s (step 1 in Figure S14a). The spin-coated SU-8 film was heated at 95 °C on a hot plate for 1 h and then kept at room temperature for 1 min for hardening. After that, the film was exposed to UV light for 20 s through a dot-patterned photomask. Cross-linking of the epoxy was carried out via postexposure baking at 65 °C for 1 min and 95 °C for 4 min, with subsequent cooling to room temperature for 1 min. During the post-exposure baking step, the dot pattern could be observed in the SU-8 film. By stirring the dot-patterned SU-8 film in the developer of 1-methoxy-2-propanol acetate solution for 30 min and rinsing with isopropyl alcohol for 10 s, the microdot-patterns were generated (step 2 in Figure S14a). Then, the PDMS solution was prepared by mixing a base (Dow Corning, Sylgard 184 A) and curing agent (Dow Corning, Sylgard B) with a mixing ratio of 10:1. The mixture was degassed for 30 min under atmospheric conditions to eliminate air bubbles and subsequently cured in a dry oven (at 65 °C) to induce cross-linking. The PDMS mixture was poured over the patterned SU-8 mold and kept in an oven at 65 °C overnight (step 3 in Figure S14a). Finally, the cured PDMS layer was peeled off from the mold to have micropillars with a height of 48 μm, diameters of 50, 70, or 120 μm, and unit cell sizes of 80 × 80, 160 × 160, or 240 × 240 μm^2, depending on the dimensions of the SU-8 dot-patterned mold (step 4 in Figure S14a). The detailed design and dimensions of the PDMS micropillars are shown in Table S1 and Figure S3. Finally, Ti/Au (5/50 nm) was deposited on PDMS micropillars to make a highly conductive layer via e-beam evaporation. E-beam evaporation was repeated twice while the PDMS pillar substrate was tilted by 45° to obtain a uniformly coated Ti/Au film over the entire pillar structure.

Growth of Polyaniline Nanofibers and Au Etching. Schematics of the growing polyaniline nanofiber layer on a PET film and the corresponding optical images are shown in Figure S14b. A 50 nm-thick Au film was deposited on a PET film (2 × 2 cm^2) using e-beam evaporation. On this Au film, polyaniline nanofibers were potentiodynamically grown at a scan rate of 100 mV s^{-1} between 0 and 0.85 V (vs. Ag/AgCl) in a solution of 0.1 m aniline monomer (99 wt %, Sigma-Aldrich) and 0.5 m sulfuric acid (H$_2$SO$_4$)(95.0%, Samchun Chemical) at room temperature: Au-deposited PET film and Ag/AgCl were used as the working electrode and the reference electrode, respectively, during the polymer growth. A platinum (Pt) electrode placed symmetrically around the working electrode was used as the counter electrode. In order to prevent the possible degradation of polyaniline, it was grown via potential cycling between 0 and 0.85 V, and taken out immediately after the end of growth cycle. After polymerization, the polyaniline nanofiber film was dried in air. The number of CV cycles was precisely controlled to obtain the desired thickness of polyaniline nanofiber film. Finally, the Au film was selectively etched using commercial gold etchant (Gold Etchant TFA, Transene Co.).

Fabrication of an Ag Nanowire Sticker. The fabrication of Ag nanowire sticker is schematically demonstrated in Figure S14c. A 50 μm thick PDMS film was formed on a silicon substrate

by spin-coating (1350 rpm, 30 s), and it was then half-cured at 65 °C for 8 min to produce a sticky film. The film was cut and transferred onto a glass substrate. Then, Ag nanowire solution (1 wt % diluted in water, Ditto technologies) with an average nanowire diameter of 65 nm and length of 10 μm was drop-casted on the half-cured PDMS film, and the Ag nanowire-embedded PDMS was dried in air.

Fabrication of the Deformable Substrate. The schematic illustration of the fabrication of the deformable substrate is shown in Figure S2. The substrate consists of three different layers marked as Layer 1, Layer 2, and Layer 3. Details of the fabrication of each layer and assembly of the three layers by injecting a liquid metal into embedded microchannels are illustrated in parts a and b, respectively, of Figure S2. The final top and side views of the substrate are also demonstrated in Figure S2c.

Two pieces of Teflon-coated stainless steel mold were employed to make "layer 1": The top mold (M1) has an array of islands with trench structures and the bottom (M2) has microchannels. PDMS was poured into M1 to fill the trench area, forming rigid islands, and the M1 was then annealed in a dry oven at 65 °C for 15 min for half-curing, which promoted bonding with the mixed polymer thin film. After half-curing, M1 with the PDMS islands and M2 were placed in contact with each other. Then, a mixed polymer of PDMS and Ecoflex with a weight-mixing ratio of 2:8 was poured into the space as thin film. The entire mold was annealed in a dry oven at 65 °C for 1 h, and the deformable substrate (layer 1) was separated from the mold where open microchannels of 500 μm were formed on the bottom surface; 1 mm-thick PDMS island arrays with a 1 mm-thick mixed thin film of PDMS and Ecoflex were formed.

The 0.7 mm-thick middle layer (layer 2) of the entire deformable substrate was made by molding. The mixed polymer of PDMS and Ecoflex was poured into the mold (M3) with microchannels of 500 μm, and it was annealed in an oven at 65 °C for 1 h. Next, the cured mixed polymer was detached from the mold to have open microchannels on the bottom surface.

A thin Ecoflex layer was spin coated at 1500 rpm for 30 s and cured at 60 °C for 1 min to make a bonding layer between layers 1 and 2.

50 *via* holes for interconnections were made by pressing the PDMS islands with a puncher (hole diameter = 0.7 mm).

The bottom layer (layer 3) was spin coated at 300 rpm for 35 s and half cured at 65 °C for 15 min in a dry oven. The assembled substrate (layers 1 and 2) was attached to layer 3.

The whole assembled substrate was cured completely in the oven at 65 °C for 30 min. As a result, a deformable substrate with embedded microchannels (width = 500 μm; depth = 500 μm) was successfully fabricated.

Finally, the liquid metal, Galinstan (68.5% Ga, 21.5% In, and 10% Sn; Rotometals), was injected through the microchannels using a microsyringe.

Characterization. Surface morphology and the cross-sectional view of the fabricated pressure sensor were investigated by taking SEM (Hitachi S-4800) and optical microscope (BX41M, Olympus) images. The attenuated total reflection Fourier transform infrared spectrum (ATR-FTIR) of the electrodeposited polyaniline nanofibers was obtained for the range of 650−4000 cm^{-1} with a resolution of 8 cm^{-1}. Raman spectral images of electrodeposited polyaniline nanofiber film were obtained (Horiba LabRam Aramis IR2), where the wavelength of the laser and the power were 532 nm and 0.5 mW, respectively. Cyclic voltammetry (CV) curves were obtained using an electrochemical analyzer (Ivium Technologies, Compact Stat). A Canon Eos-7D was used to capture the optical images. The sheet resistance of polyaniline nanofiber film was measured with a surface-resistivity meter (SRM-232) at a resolution of 0.8 Ω/sq. $I-V$ characteristics of the pressure sensor were measured using a B1500A. For the automatic and dynamic pressure measurements, a force sensor (Mark-10 Series 7, $\pm$ 0.1% accuracy) and a motion controller (SM4-0806-3S) were operated using a custom-built LabVIEW program.

CONCLUSIONS

We demonstrate the facile fabrication of a stretchable array of highly sensitive pressure sensors consisting of polyaniline nanofibers and Au-deposited PDMS micropillars. The fabricated pressure sensor showed highly reliable and stable electromechanical performance. By designing nonplanar structures for the top and bottom layers of the pressure sensor, the sensors exhibit a high sensitivity of 2.0 kPa^{-1} at a pressure below 0.22 kPa, a low detection limit of 15 Pa, a fast response time of 50 ms, and high stability over 10000 cycles with a low operating voltage of 1.0 V. The sensor also clearly detected the primary features of human-pulse waveforms from the carotid and radial artery. Furthermore, a 5 × 5 array of dry-transferred pressure sensors on our specially designed stretchable substrate could successfully detect the pressure under biaxial stretching of 15%. These results demonstrate the potential application of our stretchable pressure-sensor arrays in wearable electronic devices such as artificial skin.

Conflict of Interest: The authors declare no competing financial interest.

Supporting Information Available: The Supporting Information is available free of charge on the ACS Publications website at DOI: 10.1021/acsnano.5b03510.

Additional figures and tables (PDF)

REFERENCES AND NOTES

1. Kim, D.-H.; Lu, N.; Ma, R.; Kim, Y.-S.; Kim, R.-H.; Wang, S.; Wu, J.; Won, S. M.; Tao, H.; Islam, A.; Yu, K. J.; Kim, T.-i.; Chowdhury, R.; Ying, M.; Xu, L.; Li, M.; Chung, H.-J.; Keum, H.; McCormick, M.; Liu, P.; Zhang, Y.-W.; Omenetto, F. G.; Huang, Y.; Coleman, T.; Rogers, J. A. Epidermal Electronics. *Science* **2011**, *333*, 838−843.
2. Someya, T.; Kato, Y.; Sekitani, T.; Iba, S.; Noguchi, Y.; Murase, Y.; Kawaguchi, H.; Sakurai, T. Conformable, Flexible, Large-Area Networks of Pressure and Thermal Sensors with Organic Transistor Active Matrixes. *Proc. Natl. Acad. Sci. U. S. A.* **2005**, *102*, 12321−12325.
3. Xu, C. N.; Watanabe, T.; Akiyama, M.; Zheng, X. G. Artificial Skin to Sense Mechanical Stress by Visible Light Emission. *Appl. Phys. Lett.* **1999**, *74*, 1236−1238.
4. Park, J.; Lee, Y.; Hong, J.; Lee, Y.; Ha, M.; Jung, Y.; Lim, H.; Kim, S. Y.; Ko, H. Tactile-Direction-Sensitive and Stretchable Electronic Skins Based on Human-Skin-Inspired Interlocked Microstructures. *ACS Nano* **2014**, *8*, 12020−12029.
5. Maheshwari, V.; Saraf, R. Tactile Devices to Sense Touch on a Par with a Human Finger. *Angew. Chem., Int. Ed.* **2008**, *47*, 7808−7826.
6. Harada, S.; Honda, W.; Arie, T.; Akita, S.; Takei, K. Fully Printed, Highly Sensitive Multifunctional Artificial Electronic Whisker Arrays Integrated with Strain and Temperature Sensors. *ACS Nano* **2014**, *8*, 3921−3927.
7. Hammock, M. L.; Chortos, A.; Tee, B. C. K.; Tok, J. B. H.; Bao, Z. 25th Anniversary Article: The Evolution of Electronic Skin (E-Skin): A Brief History, Design Considerations, and Recent Progress. *Adv. Mater.* **2013**, *25*, 5997−6038.
8. Wang, C.; Hwang, D.; Yu, Z.; Takei, K.; Park, J.; Chen, T.; Ma, B.; Javey, A. User-Interactive Electronic Skin for Instantaneous Pressure Visualization. *Nat. Mater.* **2013**, *12*, 899−904.
9. Sekitani, T.; Nakajima, H.; Maeda, H.; Fukushima, T.; Aida, T.; Hata, K.; Someya, T. Stretchable Active-Matrix Organic Light-Emitting Diode Display Using Printable Elastic Conductors. *Nat. Mater.* **2009**, *8*, 494−499.

10. Pang, C.; Lee, G.-Y.; Kim, T.-i.; Kim, S. M.; Kim, H. N.; Ahn, S.-H.; Suh, K.-Y. A Flexible and Highly Sensitive Strain-Gauge Sensor Using Reversible Interlocking of Nanofibres. *Nat. Mater.* **2012**, *11*, 795–801.

11. Takahashi, T.; Takei, K.; Gillies, A. G.; Fearing, R. S.; Javey, A. Carbon Nanotube Active-Matrix Backplanes for Conformal Electronics and Sensors. *Nano Lett.* **2011**, *11*, 5408–5413.

12. Yao, H.-B.; Ge, J.; Wang, C.-F.; Wang, X.; Hu, W.; Zheng, Z.-J.; Ni, Y.; Yu, S.-H. A Flexible and Highly Pressure-Sensitive Graphene–Polyurethane Sponge Based on Fractured Microstructure Design. *Adv. Mater.* **2013**, *25*, 6692–6698.

13. Park, J.; Lee, Y.; Hong, J.; Ha, M.; Jung, Y.-D.; Lim, H.; Kim, S. Y.; Ko, H. Giant Tunneling Piezoresistance of Composite Elastomers with Interlocked Microdome Arrays for Ultra-sensitive and Multimodal Electronic Skins. *ACS Nano* **2014**, *8*, 4689–4697.

14. Tee, B. C. K.; Wang, C.; Allen, R.; Bao, Z. An Electrically and Mechanically Self-Healing Composite with Pressure- and Flexion-Sensitive Properties for Electronic Skin Applications. *Nat. Nanotechnol.* **2012**, *7*, 825–832.

15. Wang, X.; Gu, Y.; Xiong, Z.; Cui, Z.; Zhang, T. Silk-Molded Flexible, Ultrasensitive, and Highly Stable Electronic Skin for Monitoring Human Physiological Signals. *Adv. Mater.* **2014**, *26*, 1336–1342.

16. Gong, S.; Schwalb, W.; Wang, Y.; Chen, Y.; Tang, Y.; Si, J.; Shirinzadeh, B.; Cheng, W. A Wearable and Highly Sensitive Pressure Sensor with Ultrathin Gold Nanowires. *Nat. Commun.* **2014**, *5*, 3132.

17. Zhu, B.; Niu, Z.; Wang, H.; Leow, W. R.; Wang, H.; Li, Y.; Zheng, L.; Wei, J.; Huo, F.; Chen, X. Microstructured Graphene Arrays for Highly Sensitive Flexible Tactile Sensors. *Small* **2014**, *10*, 3625–3631.

18. Mannsfeld, S. C. B.; Tee, B. C. K.; Stoltenberg, R. M.; Chen, C. V. H. H.; Barman, S.; Muir, B. V. O.; Sokolov, A. N.; Reese, C.; Bao, Z. Highly Sensitive Flexible Pressure Sensors with Microstructured Rubber Dielectric Layers. *Nat. Mater.* **2010**, *9*, 859–864.

19. Lipomi, D. J.; Vosgueritchian, M.; Tee, B. C. K.; Hellstrom, S. L.; Lee, J. A.; Fox, C. H.; Bao, Z. Skin-Like Pressure and Strain Sensors Based on Transparent Elastic Films of Carbon Nanotubes. *Nat. Nanotechnol.* **2011**, *6*, 788–792.

20. Woo, S.-J.; Kong, J.-H.; Kim, D.-G.; Kim, J.-M. A Thin All-Elastomeric Capacitive Pressure Sensor Array Based on Micro-Contact Printed Elastic Conductors. *J. Mater. Chem. C* **2014**, *2*, 4415–4422.

21. Vandeparre, H.; Watson, D.; Lacour, S. P. Extremely Robust and Conformable Capacitive Pressure Sensors Based on Flexible Polyurethane Foams and Stretchable Metallization. *Appl. Phys. Lett.* **2013**, *103*, 204103.

22. Schwartz, G.; Tee, B. C. K.; Mei, J.; Appleton, A. L.; Kim, D. H.; Wang, H.; Bao, Z. Flexible Polymer Transistors with High Pressure Sensitivity for Application in Electronic Skin and Health Monitoring. *Nat. Commun.* **2013**, *4*, 1859.

23. Wu, W.; Wen, X.; Wang, Z. L. Taxel-Addressable Matrix of Vertical-Nanowire Piezotronic Transistors for Active and Adaptive Tactile Imaging. *Science* **2013**, *340*, 952–957.

24. Persano, L.; Dagdeviren, C.; Su, Y.; Zhang, Y.; Girardo, S.; Pisignano, D.; Huang, Y.; Rogers, J. A. High Performance Piezoelectric Devices Based on Aligned Arrays of Nano-fibers of Poly(Vinylidenefluoride-Co-Trifluoroethylene). *Nat. Commun.* **2013**, *4*, 1633.

25. Wang, Z. L.; Wu, W. Nanotechnology-Enabled Energy Harvesting for Self-Powered Micro-/Nanosystems. *Angew. Chem., Int. Ed.* **2012**, *51*, 11700–11721.

26. Pan, C.; Dong, L.; Zhu, G.; Niu, S.; Yu, R.; Yang, Q.; Liu, Y.; Wang, Z. L. High-Resolution Electroluminescent Imaging of Pressure Distribution Using a Piezoelectric Nanowire LED Array. *Nat. Photonics* **2013**, *7*, 752–758.

27. Fan, F.-R.; Lin, L.; Zhu, G.; Wu, W.; Zhang, R.; Wang, Z. L. Transparent Triboelectric Nanogenerators and Self-Powered Pressure Sensors Based on Micropatterned Plastic Films. *Nano Lett.* **2012**, *12*, 3109–3114.

28. Chen, J.; Zhu, G.; Yang, W.; Jing, Q.; Bai, P.; Yang, Y.; Hou, T.-C.; Wang, Z. L. Harmonic-Resonator-Based Triboelectric Nanogenerator as a Sustainable Power Source and a Self-Powered Active Vibration Sensor. *Adv. Mater.* **2013**, *25*, 6094–6099.

29. Fan, F.-R.; Tian, Z.-Q.; Lin Wang, Z. Flexible Triboelectric Generator. *Nano Energy* **2012**, *1*, 328–334.

30. Lin, L.; Xie, Y.; Wang, S.; Wu, W.; Niu, S.; Wen, X.; Wang, Z. L. Triboelectric Active Sensor Array for Self-Powered Static and Dynamic Pressure Detection and Tactile Imaging. *ACS Nano* **2013**, *7*, 8266–8274.

31. Zang, Y.; Zhang, F.; Di, C.-a.; Zhu, D. Advances of Flexible Pressure Sensors toward Artificial Intelligence and Health Care Applications. *Mater. Horiz.* **2015**, *2*, 140–156.

32. Kwon, O. K.; Lee, J. H.; Kim, K.-S.; Kang, J. W. Developing Ultrasensitive Pressure Sensor Based on Graphene Nano-ribbon: Molecular Dynamics Simulation. *Phys. E* **2013**, *47*, 6–11.

33. Shao, Q.; Niu, Z.; Hirtz, M.; Jiang, L.; Liu, Y.; Wang, Z.; Chen, X. High-Performance and Tailorable Pressure Sensor Based on Ultrathin Conductive Polymer Film. *Small* **2014**, *10*, 1466–1472.

34. Chen, M.; Duan, S.; Zhang, L.; Wang, Z.; Li, C. Three-Dimensional Porous Stretchable and Conductive Polymer Composites Based on Graphene Networks Grown by Chemical Vapour Deposition and PEDOT:PSS Coating. *Chem. Commun.* **2015**, *51*, 3169–3172.

35. Kumar, D.; Sharma, R. C. Advances in Conductive Polymers. *Eur. Polym. J.* **1998**, *34*, 1053–1060.

36. Wang, K.; Wu, H.; Meng, Y.; Wei, Z. Conducting Polymer Nanowire Arrays for High Performance Supercapacitors. *Small* **2014**, *10*, 14–31.

37. Virji, S.; Huang, J.; Kaner, R. B.; Weiller, B. H. Polyaniline Nanofiber Gas Sensors: Examination of Response Mechanisms. *Nano Lett.* **2004**, *4*, 491–496.

38. Ansari, R.; Keivani, M. B. Polyaniline Conducting Electroactive Polymers Thermal and Environmental Stability Studies. *J. Chem.* **2006**, *3*, 202–217.

39. Guo, Y.; Zhou, Y. Polyaniline Nanofibers Fabricated by Electrochemical Polymerization: A Mechanistic Study. *Eur. Polym. J.* **2007**, *43*, 2292–2297.

40. Valentová, H.; Stejskal, J. Mechanical Properties of Polyaniline. *Synth. Met.* **2010**, *160*, 832–834.

41. Yoon, J.; Hong, S. Y.; Lim, Y.; Lee, S.-J.; Zi, G.; Ha, J. S. Design and Fabrication of Novel Stretchable Device Arrays on a Deformable Polymer Substrate with Embedded Liquid-Metal Interconnections. *Adv. Mater.* **2014**, *26*, 6580–6586.

42. Meng, C.; Maeng, J.; John, S. W. M.; Irazoqui, P. P. Ultrasmall Integrated 3D Micro-Supercapacitors Solve Energy Storage for Miniature Devices. *Adv. Energy Mater.* **2014**, *4*, 1301269.

43. Yuan, L.; Xiao, X.; Ding, T.; Zhong, J.; Zhang, X.; Shen, Y.; Hu, B.; Huang, Y.; Zhou, J.; Wang, Z. L. Paper-Based Super-capacitors for Self-Powered Nanosystems. *Angew. Chem., Int. Ed.* **2012**, *51*, 4934–4938.

44. Yao, B.; Yuan, L.; Xiao, X.; Zhang, J.; Qi, Y.; Zhou, J.; Zhou, J.; Hu, B.; Chen, W. Paper-Based Solid-State Supercapacitors with Pencil-Drawing Graphite/Polyaniline Networks Hybrid Electrodes. *Nano Energy* **2013**, *2*, 1071–1078.

45. Holm, R. *Electric Contacts: Theory and Application*; Springer-Verlag: New York, 1967.

46. Chung, E.; Chen, G.; Alexander, B.; Cannesson, M. Non-Invasive Continuous Blood Pressure Monitoring: A Review of Current Applications. *Front. Med.* **2013**, *7*, 91–101.

47. Choong, C.-L.; Shim, M.-B.; Lee, B.-S.; Jeon, S.; Ko, D.-S.; Kang, T.-H.; Bae, J.; Lee, S. H.; Byun, K.-E.; Im, J.; Jeong, Y. J.; Park, C. E.; Park, J.-J.; Chung, U. I. Highly Stretchable Resistive Pressure Sensors Using a Conductive Elastomeric Composite on a Micropyramid Array. *Adv. Mater.* **2014**, *26*, 3451–3458.

48. Zhaopeng, F.; Gong, Z.; Liao, S. In Clinical Analysis for Cardiovascular Disease by Calculating Stiffness Index, Cardiac Output from Pulse Wave. *2009 Canadian Conference on Electrical and Computer Engineering*, St. John's, NL, 3−6 May 2009; IEEE, **2009**; pp 478−481.

49. V, P.; Buhutkar, P.; Bhutkar, M.; G, S. A Comparative Study of Arterial Stiffness Indices between Smokers & Non Smokers. *Int. J. Med. Res. Health Sci.* **2013**, *2*, 533–539.

50. Jung, J. H.; Lee, M.; Hong, J.-I.; Ding, Y.; Chen, C.-Y.; Chou, L.-J.; Wang, Z. L. Lead-Free NaNbO$_3$ Nanowires for a High Output Piezoelectric Nanogenerator. *ACS Nano* **2011**, *5*, 10041–10046.

51. *ABAQUS Version 6.10 User's Manual*; Hibbitt, Karlson & Sorensen: Providence, RI, 2012.